High-Performance Magnetic Sensorics for Printable and Flexible Electronics

Daniil Karnaushenko,* Denys Makarov,* Max Stöber, Dmitriy D. Karnaushenko, Stefan Baunack, and Oliver G. Schmidt

Flexible electronics has emerged as a standalone field and matured over past decades.[1–6] This alternative formulation of electronics offers the unique possibility to adjust the shape of devices at will after their fabrication. The flexibility provides vast advantages over conventional rigid electronics; flexible printed circuit (FPC) boards have become an industrial standard for consumer electronics and medical implants,[7–10] where large area, extreme thinness, and compliance to curved surfaces are the key requirements for the functional passive and active elements. Flexible devices strongly benefited from the recent developments of organic[6,11,12] as well as inorganic[10,13,14] electronics, which are prepared using printing and/or thin film technologies. Being synergetically combined with either inkjet, screen, or dispenser printing approaches, flexible electronics has witnessed fascinating innovations in several application areas including displays,[15] organic light-emitting diodes,[16] various types of sensors,[17–21] radio frequency identification tags,[22–24] and organic solar cells.[25]

To complete the family, there are strong activities toward the fabrication of flexible magnetic field sensorics envisioning active intelligent packaging, post cards, books, or promotional materials that communicate with the environment when externally triggered by a magnetic field.[14,26] By now, high-performance magnetic sensorics relying on the giant magnetoresistive (GMR) effect are prepared exclusively using thin film fabrication technologies.[14,27–33] Although this method allows fabricating extremely sensitive magnetosensorics, the economics and time efficiency for large area and high-throughput

D. Karnaushenko, Dr. D. Makarov, M. Stöber,
D. D. Karnaushenko, Dr. S. Baunack,
Prof. O. G. Schmidt
Institute for Integrative Nanosciences
Institute for Solid State and Materials Research
Dresden (IFW Dresden)
Dresden 01069, Germany
E-mail: d.karnaushenko@ifw-dresden.de; d.makarov@ifw-dresden.de
Prof. O. G. Schmidt
Material Systems for Nanoelectronics
Chemnitz University of Technology
Chemnitz 09107, Germany
Prof. O. G. Schmidt
Center for Advancing Electronics Dresden
Dresden University of Technology
Dresden 01062, Germany

preparation of magnetic functional elements for printable and flexible electronics remain an open issue. The most straightforward solution would be to print magnetic sensing elements at predefined locations on flexible circuitry. To assure applicability of the printed GMR sensors, they should provide stable response in the consumer temperature range from 0 °C up to +85 °C, which require careful optimization of the polymeric binder solution with respect to the thermal expansion coefficient. Furthermore, accounting for the relatively small amplification coefficient of available printable[12,34] and flexible[10] transistors, the relative change of the electrical resistance in the range of several tens of percent under moderate magnetic fields of about 0.5 T, provided by flexible rubber-based NdFeB permanent magnets,[35] needs to be demonstrated. Indeed, printable and flexible amplifiers exhibit a DC gain as high as 50 dB[13,36,37] and could be coupled with printable magnetoelectronics possessing magnetoresistive (MR) ratios of at least 30%. In this work, by optimizing the polymeric binder solution and the components of the magnetosensitive powder, we realize high-performance printable GMR sensorics, which fulfills the stringent thermal stability requirements of consumer electronics.

Magnetic nanoparticles surrounded by a nonmagnetic matrix reveal spin-dependent transport phenomena and hence may act as MR sensor devices,[38–41] which could be printable when immersed in a solution. Depending on the material of the interparticle matrix, different effects may occur: while the use of insulating matrices results in tunneling magnetoresistance (TMR) effect,[41–43] conducting matrices lead to the GMR effect. With respect to the former approach, only very recently, room temperature TMR was observed with a magnitude of 0.3%,[44] which is not yet fully optimized for applications in printable magnetoelectronics.

At the same time, there are strong advances in the field of GMR sensorics based on magnetic particles and operating at room temperature.[21,26,45,46] A GMR of up to 260% was reported at room temperature for granular systems consisting of carbon-coated Co nanoparticles of 18-nm diameter embedded in conductive gel-like nonmagnetic matrices.[46] The large magnitude of the GMR effect is promising to realize printable magnetic field sensors. However, the choice of gels for the conductive matrix imposes limitations on thermal stability of the sensing elements in the relevant temperature range from 0 °C up to +85 °C, as required for applications in consumer electronics. To overcome these limitations, we put forth an approach to fabricate printable magnetosensitive pastes, which were prepared using standard sputter deposition, milling, and mixing processing.[21,47] Demonstration of printing on flexible polymeric membranes potentially enables this technology to be applied in the concept of flexible electronics. However, the GMR effect of the reported printable sensors is about 7% with rather poor
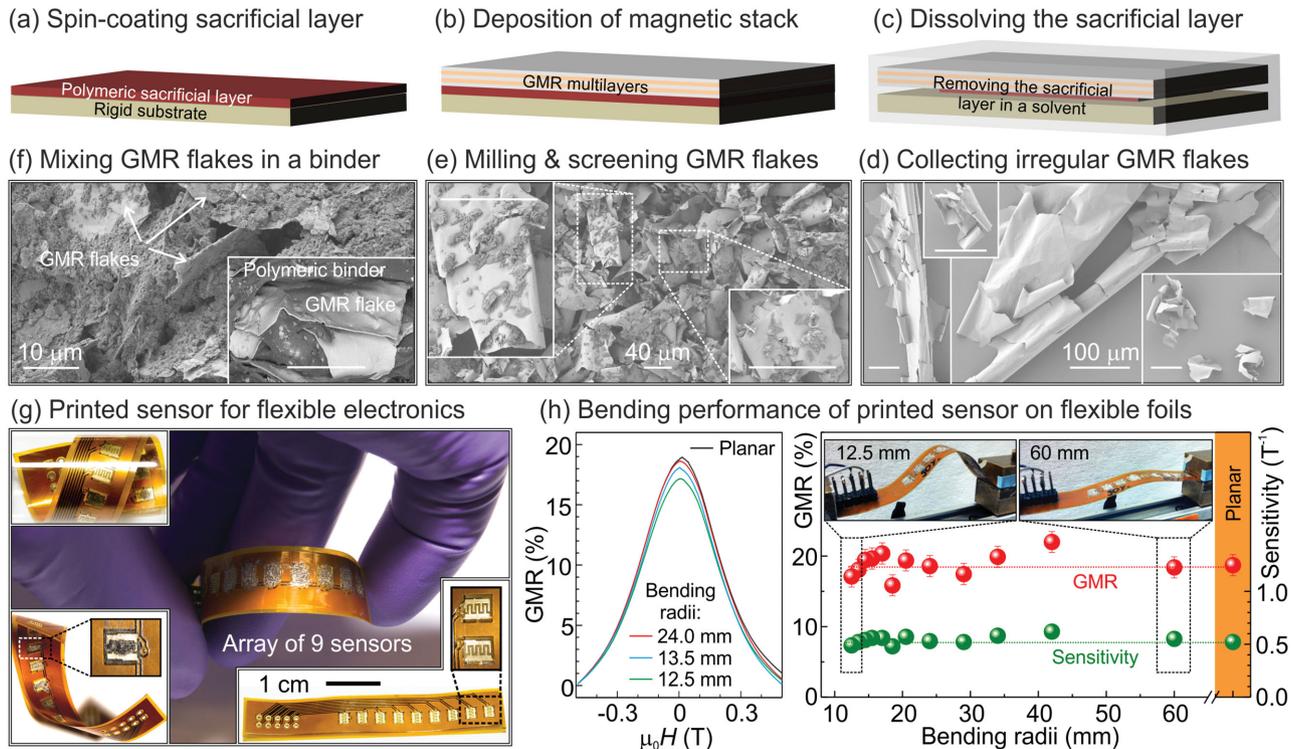
Figure 1. Schematics of the fabrication process. We start with a) spin coating the sacrificial polymeric PVC layer followed by b) the deposition of the GMR multilayer stack. c) The sacrificial layer is removed in acetone leading to the lift-off of the metal layer. d) The corresponding SEM image of the as-collected GMR flakes after the lift-off process. These metal pieces are ball milled and screened resulting in regular shaped flakes e), which are then mixed with a polymeric binder f) to prepare the GMR paste. Milling was carried out for 20 h resulting in an average flake size of (36 ± 5) μm. g) The GMR paste is applied by regular brush painting to a flexible printed circuit board to realize an array of printed GMR sensors for flexible electronics. h) The evolution of the magnetoelectrical performance of the printed sensing elements ($C_{0,GMR}$ = 90%) upon bending is investigated. The maximum sensitivity is achieved at 160 mT. The size of flakes is 150 μm; PCH polymer is used for the binder solution.

sensitivity of ≈0.06 T^{-1} and large saturation field of 2 T.[21] The rigid counterpart of the printed sensor reveals a GMR ratio of about 50% with a sensitivity of about 3 T^{-1} and a saturation field of 300 mT.[48,49]

Here, we demonstrate the very first high-performance printable magnetic field sensorics applicable for flexible electronics. Remarkably, after printing, the GMR sensor elements reveal up to 37% change of the electrical resistance in the magnetic field with a maximal sensitivity of 0.93 T^{-1} in a field of 130 mT. With this performance, the printed magnetoelectronics is comparable to reference samples prepared using standard thin film fabrication technology. Furthermore, the developed magnetosensors are fully operational in the temperature range from –10 °C up to +95 °C, which safely fulfills the requirements for consumer electronics.

The Co/Cu multilayers coupled at the 1st antiferromagnetic maximum are grown at room temperature by magnetron sputtering. The deposition is carried out onto an oxidized Si wafer with and without the spin-coated sacrificial layer. For the sacrificial layer, we chose poly(vinyl chloride-co-vinyl acetate-co-maleic acid) (PVC) as this material provides an extremely uniform surface with a roughness below 1 nm, which is crucial for fabrication of high-performance GMR sensing elements.[30] After fabrication, the material is removed without rest in acetone. Magnetoelectrical characterization of the samples prepared on the rigid wafer with and without the sacrificial polymeric layer

reveals very similar performance with a GMR ratio of about 55% and a magnetic field, which is needed to saturate the sample in the range of 300 mT (Figure S1, Supporting Information). This limits the sensitivity of the as-deposited sensors to about 4 T^{-1} in a magnetic field of 80 mT.[48] The MR ratio is defined as the magnetic field dependent change of the sample's resistance, $R(H_{ext})$, normalized to the resistance value of the magnetically saturated sample, R_{sat}: MR$(H_{ext}) = [R(H_{ext}) - R_{sat}]/R_{sat}$. The sensitivity of the sensor element is defined as the first derivative of the sample's resistance over the magnetic field divided by the resistance value: $S(H_{ext}) = [dR(H_{ext})/dH_{ext}]/R(H_{ext})$.

After deposition of the GMR multilayer stack, the samples with a sacrificial PVC layer are placed in an ultrasonically excited acetone bath leading to the complete removal of the PVC. This process results in the lift-off of the magnetosensitive stack, which is then collected and dried under ambient conditions in order to produce the GMR powder. The fabrication process is illustrated in **Figure 1**a–c. The as-collected GMR powder consists of irregular sized and shaped flakes as revealed by scanning electron microscopy (SEM) imaging (Figure 1d). To tailor the size of the GMR flakes, the powder is ball milled at a milling speed of 1200 rpm. After the ball milling process, the GMR powder is screened through appropriate silk #100 and copper #325 meshes. Analysis of the SEM image shown in Figure 1e allows to assess the lateral dimensions of the flakes; the size of the flakes is (36 ± 5) μm after 20 h of milling. About

2 h of milling is needed to fabricate the GMR powder with a flake size of (150 ±10) µm.

In order to prepare the GMR paste, the GMR powder is then mixed with a polymeric binder solution at different concentrations (Figure 1f). The binder solution consists of a polymer dissolved in a solvent. The key requirement is that the binder should provide the electrical percolation between the flakes of the printed GMR paste in the temperature range of interest. There is no theoretical approach available, which could guide us to choose a priori the "correct" polymeric binder for printable GMR sensorics. Therefore, we experimented with different polymeric binders based on PVC, polyepichlorohydrin (PCH), polychloropren (PCP), polycaprolactone (PCL), poly(acrylic acid) (PAA), and methylenebis (phenyl isocyanate)-polyester/polyether polyurethane (Pu). These polymers are dissolved in different solvents at a concentration of 40 mg/mL: PCH and PVC in acetone; PCP in cyclopentanone 66%/1-methoxy-2-propanole 34%; PAA in DI water; Pu and PCL in tetrahydrofuran (THF). The solvents should provide right viscosity as needed for a chosen printing technique, wet the surface of a recipient, and not damage the GMR flakes. Completely empirically, after screening these binders, we conclude that the best performance of printed GMR sensors is achieved in the case, when the solution is prepared based on the polymers with rather low glass transition temperature, which are dissolvable in acetone (**Figures 2** and **3**). Indeed, the use of the same solvent for storage of the GMR flakes after removal of the sacrificial layer and the binder solution allows for the continuity of the process. This aspect appeared to be crucial especially in the view that drying the GMR flakes before printing is not allowed due to their oxidation and agglomeration. The concentration of the GMR powder in the liquid binder solution, $C_{0,GMR}$, ranges from 10% to 99%, which corresponds to a content of the GMR powder in the dried binder, C_{GMR}, from 74% to 99% (Figure S2, Supporting Information).

To fabricate printed magnetosensorics for flexible electronics, the GMR paste is applied by regular brush painting to a copper-clad polyimide-based FPC board. The FPC accommodates nine independent sensor locations each consisting of a finger pattern as shown in the inset of Figure 1g. The distance between the electrodes and the width of an electrode is 250 µm. The typical thickness of the sensor is in the range of 100 µm averaged over the nine brush-painted devices. The GMR performance is evaluated by measuring changes in the electrical resistance in an applied magnetic field. The resistance is measured in the two-point configuration. A typical current strength in the order of 100 µA is supplied by a constant current source integrated in a digital multimeter Keithley 2000. An electromagnet sweeps the magnetic field up to ±650 mT. Measurements in the geometries with the magnetic field applied parallel or normal to the sensor plane revealed similar results.[21] Therefore, in the following, we will present the data taken in the geometry when the field is applied normal to the sample plane. The sensors prepared in a single run on the FPC reveal similar GMR performance as shown in Figure S3 (Supporting Information) for the case of the PAA-based binder solution.

Our study shows that there are two efficient knobs to alter the performance of the printed GMR sensors: The enhancement of the GMR ratio of the printed sensors as well as the increase
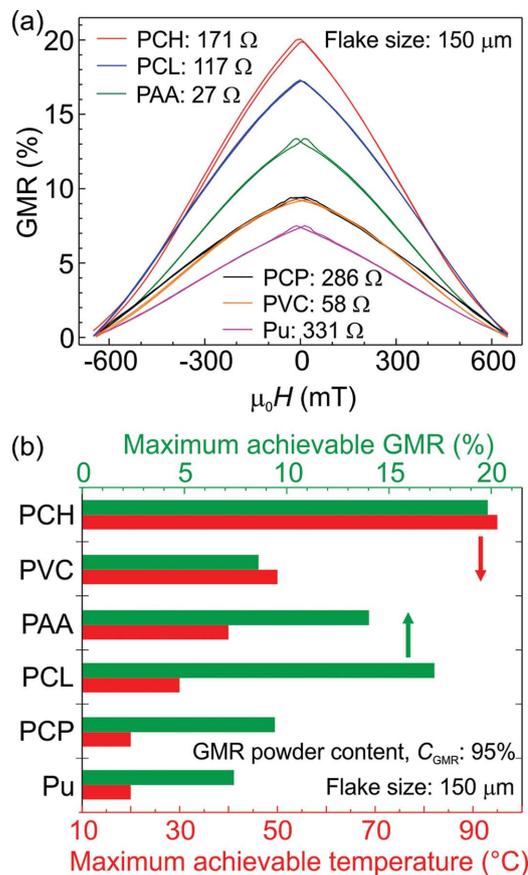

Figure 2. Impact of the polymeric binder solution on the performance of the GMR sensors printed on the FPC. The size of the GMR flakes is 150 µm; the concentration of the GMR powder in the binder is 90%. a) Magnetoelectric performance of the sensors. b) Summary of the maximum achievable GMR ratio (green bar) and operation temperature (red bar) for the sensors prepared by mixing the GMR powder with binder solutions based on different polymers.

in their sensitivity can be realized by reducing the size of the GMR flakes and/or changing the polymeric binder solution. For the latter, the characterization reveals that the choice of the polymeric binder strongly influences the GMR ratio (Figure 2a) and the operation temperature range (Figure 2b). For instance, by switching the polymer from Pu to PCH, the GMR ratio of the sensor is increased from about 7% to almost 20% keeping the same size of the GMR flakes of 150 µm. This enhancement of the GMR ratio is accompanied by a remarkable increase in the maximum achievable operation temperature from room temperature up to 95 °C.

The thermal stability of the GMR sensors printed onto FPC is evaluated by positioning them on the heating stage installed between the pole shoes of the electromagnet. The measurement is performed as follows: first, the samples are cooled down to the target temperature of −10 °C. The resistance of the sample is measured in situ while ramping the temperature at a constant speed. The time for a single cycle is about 1 h. The measurement is carried out for three to five sensors revealing good reproducibility and repeatability of the proposed approach. Independent of the chosen polymeric binder, the sensors reveal a stable response from −10 °C up to room temperature.
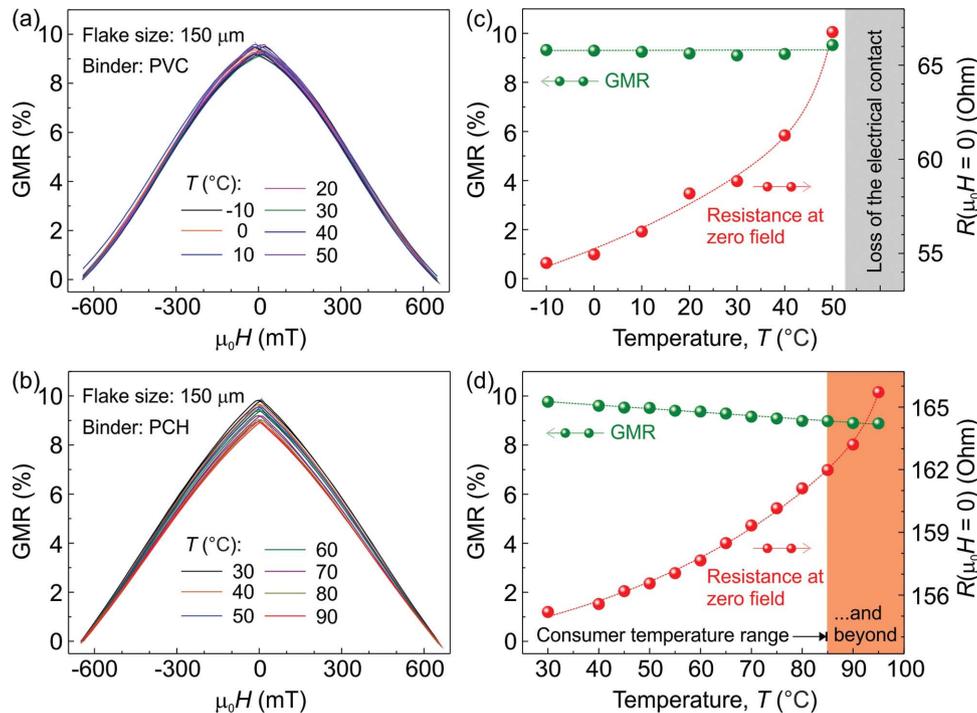
Figure 3. Change of the electrical resistance of the sensors in an applied magnetic field prepared using a) thermoplastic PVC and b) elastomer PCH. The evolution with the temperature of the electrical resistance at zero magnetic field as well as the GMR ratio is shown in panels c) for the PVC and d) for the PCH. Concentration of GMR powder in the sample is 90%; flake size is 150 μm.

However, a proper polymer has to be selected to extend the operation temperature range beyond room temperature. The optimization has to be carried out with respect to the glass transition temperature of the polymer so that no dramatic variation of any physical properties occurs within the working temperature range.

The comparison of the magnetoelectric characterization of the printed sensors prepared with binder solutions containing thermoplastic polymer (PVC) and elastomer (PCH) with a substantially different glass transition temperatures (+72 °C and –22 °C, respectively, accordingly to the datasheets of the polymers) is shown in Figure 3a,b, respectively. The performance of both printed sensors at room temperature is very similar with GMR values of about 9.5%. However, due to the strong expansion of the binder near the transition temperature, the electrical percolation between the GMR flakes embedded into the PVC binder is lost already at temperatures of about 50 °C. This is reflected in the strong increase in the sensor resistance with temperature (Figure 3c). In contrast, when the elastomer with the small transition temperature is used, operation of the printed sensor at temperatures up to 95 °C is achieved (Figure 3b,d).

Based on the results presented in Figures 2b and 3, the PCH is the most appropriate choice of the polymer to enhance the thermal stability and the GMR ratio of the sensors printed on FPCs. Interestingly, the performance of the sensors can be substantially increased even further by reducing the size of the GMR flakes and altering the concentration of the GMR powder in the polymeric binder solution (**Figure 4**). This appeared to be the key aspect to improve the sensitivity of the printed sensors. By keeping about the same concentration of the GMR powder $C_{GMR} = 90\%$, the GMR ratio is increased from 14% to 21% by

reducing the flake size from 150 to 36 μm (compare black and blue curves in Figure 4a).

We characterize the concentration dependence of the sensor performance by mixing up to 99% of the GMR powder (flake size: 36 μm) with the PCH-based binder solution. The sensors without the polymeric binder ($C_{GMR} = 100\%$) reveal rather poor adhesion to the flexible foils and therefore cannot be measured. The GMR ratio remains unchanged at a level of about 17% for the samples with a content of the GMR powder in the dry (liquid) binder of up to $C_{GMR} = 97\%$ ($C_{0,GMR} = 60\%$) (Figure 3b). For higher concentrations, a substantial increase in the GMR ratio is observed. The sample containing 99% of the GMR powder with the 36 μm flakes reveals a GMR ratio of about 37% at a saturation field of about 600 mT resulting in the maximum sensitivity of 0.93 T^{-1} at 130 mT (red curve in Figure 4a and Figure S4, Supporting Information). With this performance, the printed sensor is comparable to the reference sample before the lift-off process. The electrical resistance of the samples only slightly increases for the lower GMR powder concentration (Figure S5, Supporting Information), which is in line with the initial assumption of the percolation-driven electron transport in the system.[21]

The impact of the mechanical deformation on the magnetoelectrical response of the sensors prepared on FPC is shown in Figure 1h. The sensor is fixed at the computer-controlled bending stage (Figure S6, Supporting Information), which is located between the pole shoes of an electromagnet. At each bending radii, the complete GMR curve is measured providing access to the modification of the maximum achievable GMR ratio and the corresponding sensor sensitivity upon bending at a field parallel to sensors plane. As the sensors are prepared
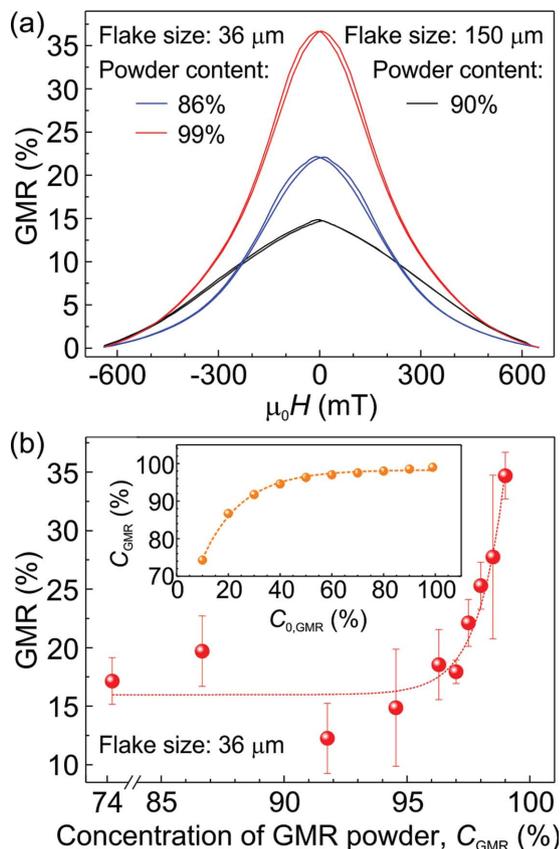
COMMUNICATION

Figure 4. a) Comparison of the GMR performance of the printed sensors with a size of flakes of 36 and 150 μm dispersed in PCH binder solution. b) The GMR response of the sensors with the concentration of the GMR powder in the binder solution. The size of flakes is 36 μm; PCH polymer is used for the binder solution.

on rather thick commercial flexible PCB supports (thickness: 180 μm), the sensor can be bent down to radii of 12 mm without sacrificing its performance and maintaining a GMR ratio of about 20% for sensors with an initial concentration of the GMR powder in a liquid binder solution $C_{0,GMR} = 90\%$ with a maximum sensitivity of (0.55 ± 0.02) T^{-1} achieved in a magnetic field of 160 mT. The bending performance of the device is mainly given by the thickness of the substrate and can be substantially improved when switching to thinner flexible foils.[6]

In conclusion, we fabricated high-performance printable magnetic field sensors relying on the GMR effect. When printed on a FPC board, the optimized magnetosensors reveal up to 37% change of the electrical resistance in the magnetic field with a maximal sensitivity of 0.93 T^{-1} at 130 mT. With these specifications, printed magnetoelectronics is comparable to state-of-the-art high-performance GMR sensors. Furthermore, the developed sensorics allows for mechanical deformations with achievable bending radii of down to 12 mm without sacrificing sensor performance. The limitation on the bending radii is imposed by the thickness of the available FPC boards but not the sensor itself. Use of thinner flexible foils should boost mechanical stability of the platform even further.[6,10,13] The key feature of the printed GMR sensors is their remarkable

temperature stability; they remain fully operational over a temperature range from –10 °C up to +95 °C, which is well beyond the requirements for consumer electronics.

With this performance, printed magnetoelectronic devices could be applied as passive components responding to a magnetic field for flexible electronics. Indeed, the output signal of the sensors can be conditioned using available printed and flexible active electronics.[13,37] In combination with flexible and printable active electronics as well as wireless communication modules,[24] the high-performance magnetic field sensorics enables realization of complex platforms capable of detecting and responding to an external magnetic field. This feature is of great interest to realize smart packaging and energy-efficient magnetic field driven switches.

Experimental Section

Preparation of the Substrate: For the deposition in a high vacuum chamber, 24 polished 3 inch naturally oxidized Si(100) wafers were used. For the first deposition run, all the wafers were cleaned in acetone, isopropanol, and DI water for 10 min with a sonication at each step. Then, for each successive deposition, the wafers were reused without additional cleaning.

Sacrificial Layer: A PVC of $M = {\approx}70\,000$ was purchased from Sigma–Aldrich Co. LLC. and dissolved in acetone at a concentration of 40 mg/mL. The solution was spin coated at 3500 rpm for 35 s on substrates and prebaked on a hot plate at 50 °C for 5 min.

Deposition of the GMR Multilayers: We chose the well-known Co/Cu GMR system coupled in the 1st AF maximum, Co(1 nm)/[Co(1 nm)/Cu(1.2 nm)]$_{50}$, due to their notorious GMR magnitude. Sputter deposition was performed in an eight target high-vacuum magnetron sputtering chamber in an argon atmosphere at room temperature simultaneously on eight wafers. The base pressure is 7×10^{-7} mbar, Ar sputter pressure: 7.5×10^{-4} mbar and the deposition rate of about 1 Å/s.

Ball Milling Process: The as-collected powder was ball milled using nonmetallic grinding balls (material: agate) using the ball milling setup (model: Pulverisette 7 by Fritsch GmbH). The diameter of the agate balls was 5 mm. The milling speed was set to 1200 rpm. A milling time of 2 (20) h was applied to achieve a size of GMR flakes of about 150 (36) μm after filtering through an appropriate silk (copper) mesh. Full width at half maximum of the distribution of the flake size is about 5%–10%.

Preparation of Binder Solution: PVC $M_w = 21\,000$ was purchased from Polysciences Europe GmbH; PCH $M_w = 700\,000$, PCP, PCL $M_w = 80\,000$, PAA $M_w = 450\,000$, and methylenebis (phenyl isocyanate)-polyester/polyether polyurethane (Pu) were purchased from Sigma–Aldrich Co. LLC. Solvents were purchased from VWR International, LLC. All of the materials were used without purification. Polymers are dissolved in different solvents at a concentration of 40 mg/mL: PCH and PVC in acetone; PCP in cyclopentanone 66%/1-methoxy-2-propanole 34%; PAA in DI water; Pu and PCL in THF.

Temperature Stability Characterization: A Peltier stage is installed between the pole shoes of an electromagnet used for the magnetoresistance characterization. The measurements were conducted in the geometry, when the magnetic field is applied perpendicular to the sample plane. The temperature can be varied in situ from –10 °C to 95 °C. The sample is attached to a copper temperature damper by a thin double-sided adhesive tape.

FPC Boards: Commercial double-sided flexible PCB substrates were designed and then ordered in LeitOn GmbH for fabrication. The average thickness of PCBs is 180 μm. The layout contains nine sensor positions. Each sensor location contains two contacts (finger pattern) of 0.25 mm width. The separation distance between the contacts is 0.25 mm (Figure S7, Supporting Information).

Supporting Information

Acknowledgements

[1] G. Gustafsson, Y. Cao, G. M. Treacy, F. Klavetter, N. Colaneri, A. J. Heeger, *Nature* **1992**, *357*, 477.

[2] J. A. Rogers, Z. Bao, K. Baldwin, A. Dodabalapur, B. Crone, V. R. Raju, V. Kuck, H. Katz, K. Amundson, J. Ewing, P. Drzaic, *Proc. Natl. Acad. Sci. USA* **2001**, *98*, 4835.

[3] J. A. Rogers, T. Someya, Y. G. Huang, *Science* **2010**, *327*, 1603.

[4] J. A. Rogers, M. G. Lagally, R. G. Nuzzo, *Nature* **2011**, *477*, 45.

[5] S. Wagner, S. Bauer, *MRS Bull.* **2012**, *37*, 207.

[6] M. Kaltenbrunner, T. Sekitani, J. Reeder, T. Yokota, K. Kuribara, T. Tokuhara, M. Drack, R. Schwodiauer, I. Graz, S. Bauer-Gogonea, S. Bauer, T. Someya, *Nature* **2013**, *499*, 458.

[7] T. Sekitani, H. Nakajima, H. Maeda, T. Fukushima, T. Aida, K. Hata, T. Someya, *Nat. Mater.* **2009**, *8*, 494.

[8] S. W. Hwang, H. Tao, D. H. Kim, H. Y. Cheng, J. K. Song, E. Rill, M. A. Brenckle, B. Panilaitis, S. M. Won, Y. S. Kim, Y. M. Song, K. J. Yu, A. Ameen, R. Li, Y. W. Su, M. M. Yang, D. L. Kaplan, M. R. Zakin, M. J. Slepian, Y. G. Huang, F. G. Omenetto, J. A. Rogers, *Science* **2012**, *337*, 1640.

[9] M. Kaltenbrunner, M. S. White, E. D. Glowacki, T. Sekitani, T. Someya, N. S. Sariciftci, S. Bauer, *Nat. Commun.* **2012**, *3*, 770.

[10] G. A. Salvatore, N. Münzenrieder, T. Kinkeldei, L. Petti, C. Zysset, I. Strebel, L. Büthe, G. Tröster, *Nat. Commun.* **2014**, *5*, 2982.

[11] T. Han, Y. Lee, M.-R. Choi, S.-H. Woo, S.-H. Bae, B. H. Hong, J.-H. Ahn, T.-W. Lee, *Nat. Photonics* **2012**, *6*, 105.

[12] K. Fukuda, Y. Takeda, M. Mizukami, D. Kumaki, S. Tokito, *Nat. Scientific Rep.* **2013**, *4*, 3947.

[13] C. Zysset, N. Münzenrieder, L. Petti, L. Büthe, G. A. Salvatore, G. Tröster, *IEEE Electron Device Lett.* **2013**, *34*, 1394.

[14] M. Melzer, D. Makarov, A. Calvimontes, D. Karnaushenko, S. Baunack, R. Kaltofen, Y. F. Mei, O. G. Schmidt, *Nano Lett.* **2011**, *11*, 2522.

[15] H. Sirringhaus, N. Tessler, R. H. Friend, *Science* **1998**, *280*, 1741.

[16] H. Uoyama, K. Goushi, K. Shizu, H. Nomura, C. Adachi, *Nature* **2012**, *492*, 234.

[17] B. Crone, A. Dodabalapur, A. Gelperin, L. Torsi, H. E. Katz, A. J. Lovinger, Z. Bao, *Appl. Phys. Lett.* **2001**, *78*, 2229.

[18] T. Someya, T. Sekitani, S. Iba, Y. Kato, H. Kawaguchi, T. Sakurai, *Proc. Nat. Acad. Sci. USA* **2004**, *101*, 9966.

[19] F. Liao, C. Chen, V. Subramanian, *Sens. Actuators B* **2005**, *107*, 849.

[20] A. Sandström, H. F. Dam, F. C. Krebs, L. Edman, *Nat. Commun.* **2012**, *3*, 1002.

[21] D. Karnaushenko, D. Makarov, C. Yan, R. Streubel, O. G. Schmidt, *Adv. Mater.* **2012**, *24*, 4518.

[22] W. Clemens, W. Fix, J. Ficker, A. Knobloch, A. Ullmann, *J. Mater. Res.* **2004**, *19*, 1963.

[23] S. Steudel, S. De Vusser, K. Myny, M. Lenes, J. Genoe, P. Heremans, *J. Appl. Phys.* **2006**, *99*, 114519.

[24] H. Kang, H. Park, Y. Park, M. Jung, B. C. Kim, G. Wallace, G. Cho, *Nat. Scientific Rep.* **2014**, *4*, 5387.

[25] A. Yella, H.-W. Lee, H. N. Tsao, C. Yi, A. Kumar Chandiran, Md. Khaja Nazeeruddin, E. W. -G. Diau, C.-Y. Yeh, S. M. Zakeeruddin, M. Grätzel, *Science* **2011**, *334*, 629.

[26] D. Makarov, D. Karnaushenko, O. G. Schmidt, *ChemPhysChem (Concept)* **2013**, *14*, 1771.

[27] G. Lin, D. Makarov, M. Melzer, W. Si, C. Yan, O. G. Schmidt, *Lab on a chip* **2014**, *14*, 4050.

[28] S. S. P. Parkin, K. P. Roche, T. Suzuki, *Jpn. J. Appl. Phys.* **1992**, *31*, L1246.

[29] S. S. P. Parkin, *Appl. Phys. Lett.* **1996**, *69*, 3092.

[30] Y.-F. Chen, Y. Mei, R. Kaltofen, J. I. Mönch, J. Schumann, J. Freudenberger, H.-J. Klauß, O. G. Schmidt, *Adv. Mater.* **2008**, *20*, 3224.

[31] C. Barraud, C. Deranlot, P. Seneor, R. Mattana, B. Dlubak, S. Fusil, K. Bouzehouane, D. Deneuve, F. Petroff, A. Fert, *Appl. Phys. Lett.* **2010**, *96*, 072502.

[32] M. Melzer, G. G. Lin, D. Makarov, O. G. Schmidt, *Adv. Mater.* **2012**, *24*, 6468.

[33] A. Bedoya-Pinto, M. Donolato, M. Gobbi, L. E. Hueso, P. Vavassori, *Appl. Phys. Lett.* **2014**, *104*, 062412.

[34] H. Yan, Z. Chen, Y. Zheng, C. Newman, J. R. Quinn, F. Dotz, M. Kastler, A. Facchetti, *Nature* **2009**, *457*, 679.

[35] http://www.rubber-magnet.com/NdFeB-flexible-magnets.htm

[36] T. Yokota, T. Sekitani, T. Tokuhara, U. Zschieschang, H. Klauk, T.-C. Huang, M. Takamiya, T. Sakurai, T. Someya, *IEEE Int. Electron Devices Meeting (IEDM)* **2011**, 14.4.1.

[37] G. Maiellaro, E. Ragonese, A. Castorina, S. Jacob, M. Benwadih, R. Coppard, E. Cantatore, G. Palmisano, *IEEE Trans. Circuits Syst.* **2013**, *60*, 3117.

[38] J. Q. Xiao, J. S. Jiang, C. L. Chien, *Phys. Rev. Lett.* **1992**, *68*, 3749.

[39] S. S. P. Parkin, *Annu. Rev. Mater. Sci.* **1995**, *25*, 357.

[40] H. Zeng, C. T. Black, R. L. Sandstrom, P. M. Rice, C. B. Murray, S. Sun, *Phys. Rev. B* **2006**, *73*, 020402(R).

[41] R. P. Tan, J. Carrey, C. Desvaux, J. Grisolia, P. Renaud, B. Chaudret, M. Respaud, *Phys. Rev. Lett.* **2007**, *99*, 176805.

[42] C. T. Black, C. B. Murray, R. L. Sandstrom, S. Sun, *Science* **2000**, *290*, 1131.

[43] R. P. Tan, J. Carrey, M. Respaud, C. Desvaux, P. Renaud, B. Chaudret, *J. Magn. Magn. Mater.* **2008**, *320*, L55.

[44] J. Dugay, R. P. Tan, A. Meffre, T. Blon, L.-M. Lacroix, J. Carrey, P. F. Fazzini, S. Lachaize, B. Chaudret, M. Respaud, *Nano Lett.* **2011**, *11*, 5128.

[45] A. Weddemann, I. Ennen, A. Regtmeier, C. Albon, A. Wolff, K. Eckstädt, N. Mill, M. K.-H. Peter, J. Mattay, C. Plattner, N. Sewald, A. Hütten, *Beilstein J. Nanotechnol.* **2010**, *1*, 75.

[46] J. Meyer, T. Rempel, M. Schäfers, F. Wittbracht, C. Müller, A. V. Patel, A. Hütten, *Smart Mater. Struct.* **2013**, *22*, 025032.

[47] D. Karnaushenko, D. Makarov, O. G. Schmidt, IFW Dresden, **2011**, Patent: DE 10 2011 077 907.8.

[48] M. Melzer, D. Karnaushenko, D. Makarov, L. Baraban, A. Calvimontes, I. Monch, R. Kaltofen, Y. F. Mei, O. G. Schmidt, *RSC Adv.* **2012**, *2*, 2284.

[49] M. Melzer, A. Kopylov, D. Makarov, O. G. Schmidt, *SPIN* **2013**, *3*, 6.